Random Wave Measurements in Front of Reflective Structures

By Gert Klopman[1] and Jentsje W. van der Meer[2]

Abstract: The changes in the wave spectrum and significant wave height near a reflective structure are investigated. Significant wave-height measurements with a one wave gauge show a standing wave pattern near the structure, extending offshore to about two times the spectral-peak wavelength for a JONSWAP incidental wave spectrum. The measured spectra also reveal a pattern of nodal and antinodal frequencies, even to much larger distances from the structure. These findings are in agreement with results from linear wave theory. Multigauge techniques can be used to discriminate between incident and reflected waves. Despite the standing wave pattern these techniques can be used to determine the incident wave height accurately up close to the structure—the distance being limited by the extend of the evanescent wave modes attached to the structure.

INTRODUCTION

In the design of coastal structures laboratory experiments are frequently used to determine the loading on or damage to a structure due to the incident waves. Because real sea waves are of a random nature, laboratory experiments with random wave loading are preferred increasingly more over regular wave testing.

For the interpretation of the laboratory results it is important to know the incident wave conditions near the structure. This is because a relationship is sought between the loading (i.e., incident wave conditions) and the response of the structure. The wave conditions are also needed to be able to compare with previous experience and literature. If a part of the bathymetry in front of the structure is also modeled, it is desirable to measure the wave conditions as close to the structure as possible. In the present paper we address the problem of how to locate wave measurements near the structure in a sensible way.

Because most structures are reflective, standing waves will occur. For regular waves a pattern of nodes and antinodes in the wave height is found extending over the whole area in front of the structure. However, for random waves the significant wave height only shows as a standing wave pattern close to the structure. This is due to the difference in the nodal and antinodal frequencies in the spectrum at a certain location. Only close to the structure do nodes and antinodes in the spectrum vary slowly with frequency, also producing nodes and antinodes in the significant wave height. Far away from the structure the nodal frequencies become very dense, resulting in a grassy shape of the spectrum. However, the total wave energy is nearly constant, producing a constant significant wave height. The distance over which the significant wave height oscillates depends on the shape of the incident wave spectrum and the reflection coefficient of the structure. In the present paper we consider this in more detail with the aid of linear wave theory.

The results of detailed random wave measurements are discussed, with wave elevations measured at 37 locations in front of a rubble-mound breakwater and a vertical wall. Wave spectra and significant wave heights were determined, as well as incident and reflected waves using a multigauge technique [see, e.g., Goda and Suzuki (1976), Mansard and Funke (1980), and Zelt and Skjelbreia (1992)]. Comparisons of the measurement results with linear wave theory are discussed.

[1]Sr. Res. Engr., Albatros Flow Research, P.O. Box 85, NL-8325ZH Vollenhove, The Netherlands; formerly, Delft Hydraulics, P.O. Box 177, NL-2600MH Delft, The Netherlands. E-mail: Gert.Klopman@afr.nl

[2]Head Water Defences, INFRAM, P.O. Box 81, NL-3890AB Zeewolde, The Netherlands; formerly, Delft Hydraulics, P.O. Box 177, NL-2600MH Delft, The Netherlands. E-mail: jentsje.vandermeer@infram.nl

Note. Discussion open until July 1, 1999. To extend the closing date one month, a written request must be filed with the ASCE Manager of Journals. The manuscript for this paper was submitted for review and possible publication on June 5, 1995. This paper is part of the ***Journal of Waterway, Port, Coastal, and Ocean Engineering***, Vol. 125, No. 1, January/February, 1999. ©ASCE, ISSN 0733-950X/99/0001-0039–0045/ $8.00 + $.50 per page. Paper No. 10853.

REFLECTION ACCORDING TO LINEAR WAVE THEORY

Regular Waves

Let us consider a structure and foreland that are uniform alongshore, under the attack of uniform incident regular waves of a fixed frequency f. The cross-shore coordinate is denoted by x and the alongshore coordinate is called y, with the origin located near the structure and the positive x-direction in the offshore direction (Fig. 1). The water depth is denoted by $h(x)$.

The waves will refract and shoal over the foreland, reflect against the structure, and undergo inverse refraction and shoaling as they travel away from the structure. According to linear wave theory, the incident and reflected wave rays make an equal angle θ_0 with the x-direction (which is normal to the structure). Also the refraction of the reflected wave will be symmetrical with respect to the refraction of the incident wave. Therefore the wave rays of the incident and the reflected waves are symmetrical with respect to the x-axis (Fig. 1).

We will present only the resulting expressions for the refraction of the incident wave over the foreland. [A detailed description of wave refraction can be found, for instance, in Dingemans (1994, Section 2.3).] The free-surface elevation $\eta(x, y, t)$ of the incident wave can be described by

$$\eta(x, y, t) = \text{Re } a(x)e^{i\psi(x,y,t)} \tag{1}$$

where $a(x)$ = wave amplitude; $\psi(x, y, t)$ = wave phase; t = time; $i = \sqrt{-1}$; and Re denoting that the real part should be taken of the following expression. By definition, the x- and y-components of the wave-number vector (k_x, k_y) and the frequency f are related to the wave phase $\psi(x, y, t)$ by

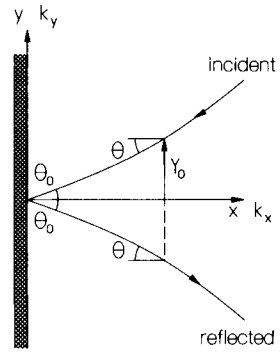

FIG. 1. Definition Sketch of Wave Refraction and Reflection

$$k_x \equiv \frac{\partial \psi}{\partial x}; \quad k_y \equiv \frac{\partial \psi}{\partial y}; \quad 2\pi f \equiv -\frac{\partial \psi}{\partial t} \qquad (2a-c)$$

In our case the frequency f is constant, and k_x and k_y are only functions of x, so that the wave phase of the incident wave becomes

$$\psi(x, y, t) = \int_{x_i}^{x} k_x(x')\, dx' + k_y(x)y - 2\pi f t \qquad (3)$$

where $(x_i, 0)$ = location at which the incident waves are specified. According to linear wave theory, the length of the wave-number vector $k = \sqrt{k_x^2 + k_y^2}$ is related to the frequency f by the dispersion relation

$$(2\pi f)^2 = gk(x)\tanh[k(x)h(x)] \qquad (4)$$

where g = gravitational acceleration constant. When the angle between the wave propagation direction and the negative x-direction is denoted by $\theta(x)$ (Fig. 1) then the wave-number vector can be written as $(k_x, k_y) = (-k \cos \theta, -k \sin \theta)$.

The variation of the angle $\theta(x)$ along a ray due to refraction can then be described by Snel's law

$$k(x)\sin \theta(x) = -k_y = \text{constant} \qquad (5)$$

Using simple goniometry, k_x is related to k and k_y by

$$k_x(x) = -k \cos \theta(x) = -\sqrt{k^2(x) - k_y^2} \qquad (6)$$

Then the y-coordinates $Y(x)$ of a ray passing through a point (x_i, y_i) are related to the x-coordinates by

$$Y(x) = y_i + \int_{x_i}^{x} \frac{dY(x')}{dx'}\, dx' = y_i + \int_{x_i}^{x} \frac{k_y}{k_x(x')}\, dx'$$

$$= y_i - \int_{x_i}^{x} \frac{k_y}{\sqrt{k^2(x') - k_y^2}}\, dx' \qquad (7)$$

For an incident wave ray passing through the origin, the ray path is described by

$$Y_0(x) = -\int_0^x \frac{k_y}{\sqrt{k^2(x') - k_y^2}}\, dx' \qquad (8)$$

where it should be remembered that $k_y = -k \sin \theta$ is negative for the incident waves traveling in the negative x-direction.

The phase difference $\Delta\psi_h$ between the origin and a point $(x, Y_0(x))$ is found by using (3), (6), and (8)

$$\Delta\psi_h(x) = \psi(0, 0, t) - \psi(x, Y_0(x), t) = \int_x^0 k_x(x')\, dx' - k_y Y_0(x)$$

$$= \int_0^x \frac{k^2(x')}{\sqrt{k^2(x') - k_y^2}}\, dx' \qquad (9)$$

An incident wave passing through the point $(x, Y_0(x))$ reflects at the origin and the reflected wave passes through $(x, -Y_0(x))$. The phase difference that the wave undergoes while traveling over the foreland is thus equal to $2\Delta\psi_h(x) + \Delta\psi_r$, with $\Delta\psi_r$ the extra phase difference experienced during reflection against the structure.

At $(x, -Y_0(x))$ two wave systems are present traveling in different directions: An incident wave and a reflected wave originating from the point $(x, Y_0(x))$. Using (3) the phase difference between incident waves at $(x, -Y_0(x))$ and $(x, Y_0(x))$ is found to be equal to

$$\Delta\psi_y(x) = \psi(x, Y_0(x), t) - \psi(x, -Y_0(x), t)$$

$$= -2\int_0^x \frac{k_y^2}{\sqrt{k^2(x') - k_y^2}}\, dx' \qquad (10)$$

Therefore, the total phase difference $\Delta\psi(x)$ between the incident and reflected wave becomes

$$\Delta\psi(x) = 2\Delta\psi_h(x) + \Delta\psi_r + \Delta\psi_y(x)$$

$$= \Delta\psi_r + 2\int_0^x \sqrt{k^2(x') - k_y^2}\, dx' \qquad (11)$$

For phase differences $\Delta\psi(x) = 0, \pi, 2\pi, \ldots$ antinodes in the wave height will occur, and for $\Delta\psi(x) = (1/2)\pi, (3/2)\pi, (5/2)\pi, \ldots$ there will be nodes.

Assume that the structure has a complex-valued reflection coefficient R, which can be written in exponential form as

$$R = |R|e^{i\Delta\psi_r} \qquad (12)$$

where $|R|$ = ratio of the reflected to the incident wave height; and $\Delta\psi_r$ = phase shift during reflection. Then the total surface elevation $\zeta(x, y, t)$, which consists of the incident wave $\eta(x, y, t)$ and the reflected wave, becomes with the aid of (11) and (12)

$$\zeta(x, y, t) = \text{Re } K_r(x)\eta(x, y, t) = \text{Re } K_r(x)a(x)e^{i\psi(x,y,t)} \qquad (13a)$$

$$K_r(x) = 1 + |R|\exp\left(i\Delta\psi_r + 2i\int_0^x \sqrt{k^2(x') - k_y^2}\, dx'\right) \qquad (13b)$$

Shoaling has no effect, because the relative amount of incident wave shoaling is equal to the relative amount of the reflected wave deshoaling. The relative wave height variation in the x-direction is found by taking the absolute value $|K_r|(x)|$ from (13b)

$$|K_r(x)|^2 = 1 + |R|^2 + 2|R|\cos\left(\Delta\psi_r + 2\int_0^x \sqrt{k^2(x') - k_y^2}\, dx'\right) \qquad (14)$$

For the special case of a horizontal bottom $h(x) = h_0$ the wave number k and the incident wave angle θ will also be constants and thus

$$|K_r(x)|^2 = 1 + |R|^2 + 2|R|\cos(\Delta\psi_r + 2kx \cos \theta) \qquad (15)$$

Random Waves

Multidirectional random waves are assumed to be an ergodic Gaussian random process. They are characterized by the autospectral density function $S_{\zeta\zeta}(f, \theta; x)$ (in the remainder abbreviated to spectrum) of the water surface elevation $\zeta(x, y, t)$. The incident wave spectrum is denoted as $S_{\eta\eta}(f, \theta; x)$. The wave spectrum $S_{\zeta\zeta}(f, \theta; x)$ is determined from the incident wave spectrum $S_{\eta\eta}(f, \theta; x)$ by using the refraction and reflection transfer function $|K_r(f, \theta; x)|^2$

$$S_{\zeta\zeta}(f, \theta; x) = |K_r(f, \theta; x)|^2 S_{\eta\eta}(f, \theta; x) \qquad (16)$$

with $|K_r(f, \theta; x|^2$ given by (14), but now with parameters depending also on frequency and incident wave angle

$$|K_r(f, \theta; x)|^2 = 1 + |R(f, \theta_0)|^2 + 2|R(f, \theta_0)|\cos$$

$$\cdot\left(\Delta\psi_r(f, \theta_0) + 2\int_0^x \sqrt{k^2(f; x') - k_y^2(f, \theta; x)}\, dx'\right) \qquad (17)$$

where θ_0 = angle of incidence at $x = 0$ of the wave ray with the structure normal. The wave number k at each frequency f and depth $h(x)$ is again given by the dispersion relation (4).

For completeness, we give the expressions for shoaling and refraction of the incident multidirectional random waves [e.g., Le Méhauté and Wang (1982)]

$$c(f; x_1)c_g(f; x_1)S_{\eta\eta}(f, \theta_1; x_1) = c(f; x_2)c_g(f; x_2)S_{\eta\eta}(f, \theta_2; x_2)$$

$$= \text{constant} \tag{18a}$$

$$k(f; x_1)\sin\theta_1 = k(f; x_2)\sin\theta_2 = \text{constant} \tag{18b}$$

where $c(f; x) \equiv 2\pi f/k(x)$ = wave celerity; and $c_g(f; x) \equiv 2\pi[\partial f(k, h)/\partial k]$ = group velocity obtained by differentiating the dispersion relation [(4)] with respect to the wave number k.

For a horizontal bottom $h(x) = h_0$, the waves do not shoal or refract, and so the wave rays are straight lines with $k(f)$ and θ constants. Then the transfer function $|K_r(f, \theta; x)|^2$ between incident and total wave spectrum becomes

$$|K_r(f, \theta; x)|^2 = 1 + |R(f, \theta)|^2 + 2|R(f, \theta)|$$

$$\cdot\cos[\Delta\psi_r(f, \theta) + 2k(f)x\cos\theta] \tag{19}$$

Because there is no refraction and shoaling, the incident wave spectrum $S_{\eta\eta}(f, \theta)$ is independent of the position (x, y).

Another case is long-crested random waves at normal incidence, which is the situation encountered in laboratory wave channels. The corresponding transfer function between incident wave spectrum $S_{\eta\eta}(f; x)$ and total wave spectrum $S_{\zeta\zeta}(f; x)$ is

$$|K_r(f; x)|^2 = 1 + |R(f)|^2 + 2|R(f)|$$

$$\cdot\cos\left[\Delta\psi_r(f) + 2\int_0^x k(f; x')\,dx'\right] \tag{20}$$

and wave shoaling is now described as

$$c_g(f; x_1)S_{\eta\eta}(f; x_1) = c_g(f; x_2)S_{\eta\eta}(f; x_2) = \text{constant} \tag{21}$$

which is obtained from a careful integration of the multidirectional wave shoaling relation [(18a)] along lines of constant $k_x(f, \theta; x) = k(f; x)\cos\theta$.

An example of a total wave spectrum $S_{\zeta\zeta}(f; x)$ due to a JONSWAP incident wave spectrum $S_{\eta\eta}(f; x)$ is shown in Fig. 2. In this and all subsequent examples the waves reflect against a perfectly reflecting vertical wall with $|R(f, \theta)| = 1$ and $\Delta\psi_r(f, \theta) = 0$, and the waves travel over a horizontal bottom with a relative water depth of $h_0/(gT_p^2) = 0.0125$. Unless stated otherwise, the incident wave spectrum is of JONSWAP shape with peakedness factor $\gamma = 3.3$. In Fig. 2 it can be observed that $S_{\zeta\zeta}(f; x)$ contains nodal and antinodal frequencies and that the distance in the frequency domain between adjacent spectrum nodes reduces when moving offshore. This nodal-frequency concentration for increasing x can be explained by observing that a node occurs if

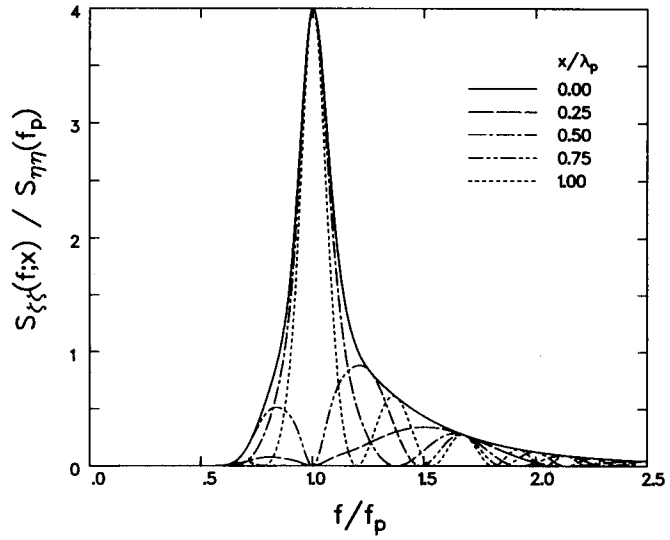

FIG. 2. Wave Spectra $S_{\zeta\zeta}(f; x)/S_{\eta\eta}(f_p)$ as Function of f/f_p at Locations $x/\lambda_p = 0$, 0.25, 0.50, 0.75, and 1; for $\bar{\theta} = 0°$ and $\sigma = 0°$

$$x = \left(\frac{1}{4} + \frac{1}{2}n\right)\frac{c(f)}{f}, \quad \text{for } n = 1, 2, 3, \ldots \tag{22}$$

for the case of a horizontal bottom. So the distance between two nodal frequencies f_1 and f_2 is equal to

$$f_2 - f_1 = \frac{1}{x}\left[\left(\frac{1}{4} + \frac{1}{2}n_2\right)c(f_2) - \left(\frac{1}{4} + \frac{1}{2}n_1\right)c(f_1)\right] \tag{23}$$

which is seen to be inverse proportional to x. Because $c(f)$ is a monotonic decreasing function of f, it can also be easily verified that $|f_2 - f_1|$ for given n_1 and n_2 always decreases in the offshore direction. This behavior can also be observed in Fig. 2.

Significant Wave Height

Let us now consider the wave-height variation in front of the structure. The significant wave height H_{m_0} is defined as

$$H_{m_0}(x) \equiv 4\sqrt{m_0(x)} \tag{24}$$

where $m_0(x)$ = total variance of the wave field

$$m_0(x) = \int_{-\pi}^{+\pi}\int_0^\infty S_{\zeta\zeta}(f, \theta; x)\,df\,d\theta \tag{25}$$

Another representation of the wave field statistics is by using the wave-number spectrum $\Phi_{\eta\eta}(k, \theta; x)$ instead of the frequency spectrum $S_{\eta\eta}(f, \theta; x)$. These two representations are related by [see, e.g., Le Méhauté and Wang (1982)]

$$\Phi_{\eta\eta}(k, \theta; x) = \frac{1}{2\pi}c_g(f; x)S_{\eta\eta}(f, \theta; x) \tag{26}$$

due to the fact that corresponding areas in (k, θ) and (f, θ) space should contain the same amount of wave energy.

To get a feeling for the behavior of $H_{m_0}(x)$, we first study the special case of long-crested incident waves over a horizontal bottom. Assume that $|R|$ is a constant independent of frequency and that the phase difference due to reflection is equal to zero. The following analysis can easily be extended to phase differences varying linearly with the wave number k. The incident spectra $S_{\eta\eta}(f, \theta)$ and $\Phi_{\eta\eta}(f, \theta)$ for long-crested waves traveling under an angle θ_L with the x-direction are

$$S_{\eta\eta}(f, \theta) = S_{\eta\eta}(f)\delta(\theta - \theta_L) \tag{27a}$$

$$\Phi_{\eta\eta}(k, \theta) = \Phi_{\eta\eta}(k)\delta(\theta - \theta_L) \tag{27b}$$

where $S_{\eta\eta}(f)$ and $\Phi_{\eta\eta}(k)$ = one-dimensional spectra; and $\delta(x)$ = Kronecker-delta function [i.e., $\delta(x) = 1$ for $x = 0$ and $\delta(x) = 0$ for all other x]. Note that the spectra are independent of x due to the horizontal bottom. The transfer function $|K_r(f, \theta; x)|^2$ is given by (19) and so we have for $m_0(x)$

$$m_0(x) = \int_0^\infty \{1 + |R|^2 + 2|R|\cos[2k(f)x\cos\theta_L]\}S_{\eta\eta}(f)\,df$$

$$= \int_0^\infty \{1 + |R|^2 + 2|R|\cos[2kx\cos\theta_L]\}\Phi_{\eta\eta}(k)\,dk$$

$$= (1 + |R|^2)\Gamma_{\eta\eta}(0) + 2|R|\Gamma_{\eta\eta}(2x\cos\theta_L) \tag{28}$$

with the spatial autocovariance $\Gamma_{\eta\eta}(x)$ defined by

$$\Gamma_{\eta\eta}(x) \equiv \int_0^\infty \Phi_{\eta\eta}(k)\cos(kx)\,dk \tag{29}$$

where $\Gamma_{\eta\eta}(x)$ = Fourier transform of $\Phi_{\eta\eta}(k)$. The incident waves have a significant wave height $H_{m_0,i} = 4\sqrt{\Gamma_{\eta\eta}(0)}$ and therefore the ratio between measured and incident wave height at a certain location (x, y) becomes, for long-crested random waves over a horizontal bottom

$$\frac{H_{m_0}(x)}{H_{m_0,i}} = [(1 + |R|^2) + 2|R|C_{\eta\eta}(2x \cos \theta_L)]^{1/2} \quad (30)$$

where $C_{\eta\eta}(x) \equiv \Gamma_{\eta\eta}(x)/\Gamma_{\eta\eta}(0)$ = spatial autocorrelation function. Because at $x = 0$ the autocorrelation $C_{\eta\eta}(0) = 1$ we have at the structure $H_{m_0}(0) = (1 + |R|)H_{m_0,i}$. Far away from the structure the autocorrelation will go to zero, and so at infinity we find $H_{m_0}(\infty) = \sqrt{1 + |R|^2}H_{m_0,i}$. How fast the wave height approaches this limit depends on the angle θ_L and the form of $C_{\eta\eta}(x)$. The latter is completely determined by the shape of the incident wave spectrum: Narrow-banded spectra will result in a spatial autocorrelation $C_{\eta\eta}(x)$ that will approach slower to zero and with more oscillations than for a broad-banded spectrum. An example of the influence of the spectrum width is shown in Fig. 3, comparing the theoretical significant wave-height variation of a narrow-banded (JONSWAP) and a broad-banded (Pierson-Moskowitz) spectrum. The oscillations in the significant wave height of the Pierson-Moskowitz spectrum damp much stronger than the ones for the JONSWAP spectrum. Furthermore it is clear from (30) that angles of incidence θ_L unequal to zero will produce a standing significant wave pattern extending over a larger area than waves of normal incidence (Fig. 3).

The influence of multidirectionality is also investigated for

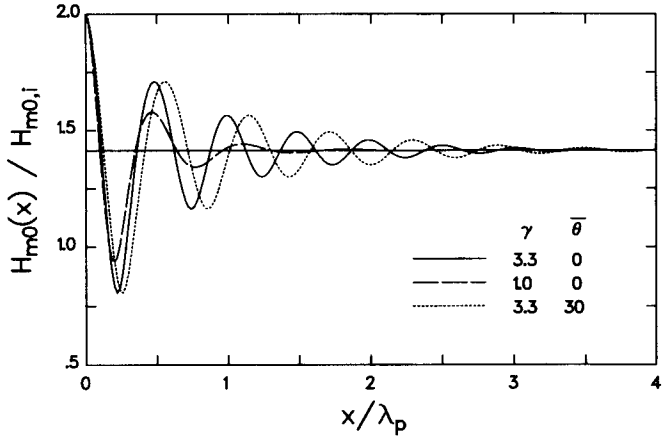

FIG. 3. Influence of Spectrum Width and Angle of Incidence on $H_{m_0}(x)/H_{m_0,i}$ as Function of x/λ_p. γ = 3.3: JONSWAP Incident Wave Spectrum; γ = 1.0: Pierson-Moskowitz Incident Wave Spectrum; and Long-Crested Waves (σ = 0°), Angles in Degrees

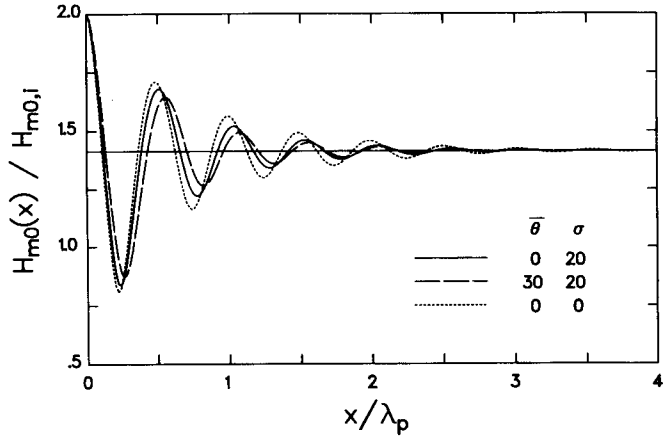

FIG. 4. Influence of Directional Spread on $H_{m_0}(x)/H_{m_0,i}$ as Function of x/λ_p. Angles in Degrees

waves over a horizontal bottom. The wave directional-spreading function $D(\theta)$ is assumed to be independent of the frequency f

$$S_{\eta\eta}(f, \theta) = S_{\eta\eta}(f)D(\theta); \quad \Phi_{\eta\eta}(k, \theta) = \Phi_{\eta\eta}(k)D(\theta) \quad (31a,b)$$

where $D(\theta)$ is assumed to be shaped like the Gaussian distribution

$$D(\theta) = \frac{1}{\sqrt{2\pi}\sigma} \exp\left[-\frac{1}{2}\left(\frac{\theta - \bar{\theta}}{\sigma}\right)^2\right] \quad (32)$$

where $\bar{\theta}$ = mean incident wave-propagation direction; and σ = directional-spreading standard deviation. To have $\int_{-\pi}^{+\pi} D(\theta)\, d\theta \approx 1$ the spreading parameter σ should not be too large (i.e., $\sigma < \pi/3$). Then the variance $m_0(x)$ becomes

$$m_0(x) = (1 + |R|^2)\Gamma_{\eta\eta}(0) + 2|R| \int_0^\infty \Phi_{\eta\eta}(k)F(kx; \bar{\theta}, \sigma)\, dk \quad (33)$$

where

$$F(kx; \bar{\theta}, \sigma) = \int_{\bar{\theta}-\pi}^{\bar{\theta}+\pi} \frac{1}{\sqrt{2\pi}\sigma} \exp\left[-\frac{1}{2}\left(\frac{\theta - \bar{\theta}}{\sigma}\right)^2\right] \cdot \cos(2kx \cos \theta)\, d\theta \quad (34)$$

This integral can be approximated very well by using a second-order Taylor-series expansion of cos θ around $\bar{\theta}$

$$\cos \theta \simeq \cos \bar{\theta} - (\theta - \bar{\theta})\sin \bar{\theta} - \frac{1}{2}(\theta - \bar{\theta})^2 \cos \bar{\theta} \quad (35)$$

and by extending the integration limits to minus and plus infinity. The resulting approximation of $F(kx; \bar{\theta}, \sigma)$ is [see, e.g., Gradshteyn and Ryzhik (1980, Eq. 3.923.2)]

$$F(kx; \bar{\theta}, \sigma) \simeq \frac{1}{\sqrt[4]{1 + \mu^2}} \exp\left(-\frac{\nu^2}{1 + \mu^2}\right) \cdot \cos\left[\frac{\mu}{2\sigma^2}\left(2 + \frac{\nu^2}{1 + \mu^2}\right) - \frac{1}{2}\arctan \mu\right] \quad (36)$$

where $\mu = 2kx\sigma^2 \cos \bar{\theta}$ and $\nu = 2kx\sigma^2 \sin \bar{\theta}$.

As an example, the significant wave-height variation for two JONSWAP incident wave spectra of normal incidence ($\bar{\theta}$ = 0°), a long-crested one (σ = 0°) and a short-crested one (σ = 20°) are shown in Fig. 4 for a fully reflective structure. The significant wave-height variation reduces a bit faster to the asymptotic value for the short-crested waves than for the long-crested waves.

As Fig. 4 shows, the significant wave height of multidirectional waves under an angle $\bar{\theta}$ = 30° can approach the asymptotic value even faster than for the same waves under normal incidence ($\bar{\theta}$ = 0°), which is in contrast with the findings for long-crested waves (shown in Fig. 3).

For the case of a reflective structure and long-crested random waves of normal incidence, Hughes (1992) studied the behavior of the root-mean-square near-bottom velocity oscillations, which is another frequency-averaged parameter just like the significant wave height.

EXPERIMENTAL SETUP

The experiments were performed in a glass-walled wave channel. The channel has a length of 45 m and a width of 1.00 m. The reflective structure was located at the end of a smooth concrete 1:50 slope in 0.50 m of water depth (Fig. 5). The horizontal 0.90-m-deep part of the channel extended from the wavemaker to the start of the 1:50 slope. Two reflective structures were tested: (1) A vertical wall; and (2) a rubble-mound breakwater with a front slope of 1:1.5. The original x

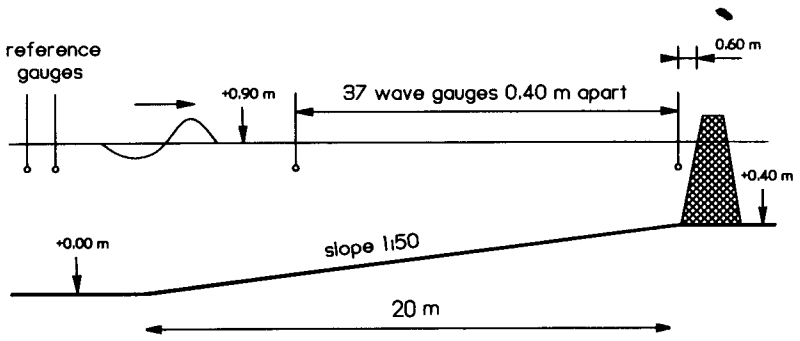

FIG. 5. Experimental Setup

TABLE 1. Test Conditions

Test (1)	Structure (2)	$H_{m_0,i}$ (m) (3)	T_p (s) (4)	s_{op} (5)	λ_p (m) (6)	$\bar{R}$ (7)
1	Vertical wall	0.156	1.49	0.04	2.80	0.89
2	Vertical wall	0.158	2.16	0.02	4.44	0.92
3	Breakwater	0.209	1.79	0.04	3.55	0.28
4	Breakwater	0.206	2.49	0.02	5.22	0.44

= 0 is located at the intersection of the still-water elevation with the front face of the structure.

The random waves were generated by a piston-type translating wave board, controlled by a computer. To prevent reflected waves to re-reflect against the wave board, an active wave-absorption system on the wave board was used. Incident random waves were generated according to a JONSWAP spectrum, with a peakedness factor $\gamma = 3.3$

For each structure the wave fields due to two different incident wave conditions were measured: One with a wave steepness $s_{op} = 0.02$ and another with $s_{op} = 0.04$. The wave steepness s_{op} is defined as $s_{op} \equiv 2\pi H_{m_0,i}/(gT_p^2)$, with $T_p = 1/f_p$ and f_p is the spectral-peak frequency. The test conditions are given in Table 1, where λ_p is the wave length associated with T_p and in 0.50 m of water depth. The test duration was ~1,000 mean wave periods.

The free-surface water elevations were measured at 39 locations by using 22 resistance-type wave gauges: Each test run was repeated with 17 of the 22 wave gauges moved to another location. Two wave gauges in the 0.90-m-deep horizontal part of the wave channel were not moved and were used to determine the incident wave conditions. Three gauges on the slope were not moved to establish an overlap between the two runs, so there were 37 measuring locations on the slope in front of the structure (Fig. 5). For the breakwater tests, the first gauge was located near the toe at 0.60 m from the intersection of the still-water level with the breakwater. For the tests with a vertical wall the first wave gauge was 0.22 m from the front of the wall, and the second 0.38 m. The remaining locations on the slope were spaced 0.4 m apart. The instruments were sampled with 25 Hz for ~1,000 mean wave periods.

RESULTS AND ANALYSIS

To determine the spatial variation of the significant wave height $H_{m_0}(x)$ near the structure, the wave spectra $S_{\zeta\zeta}(f; x)$ and significant weight height $H_{m_0}(x)$ for each of the 37 wave gauges on the slope were determined. The two reference gauges were used to determine the incident wave spectrum $S_{\eta\eta}(f; \infty)$ on the horizontal bottom part, as well as $H_{m_0,i}(\infty)$, using the method of Goda and Suzuki (1976). Also the frequency-averaged reflection coefficient $\bar{R}(\infty)$ was determined

$$\bar{R}(x) = \left(\int_0^\infty \frac{S_{\zeta\zeta}(f; x)}{S_{\eta\eta}(f; x)}\, df - 1 \right)^{1/2} \tag{37}$$

For computed reflection coefficients $\bar{R}(\infty)$ are given in Table 1. It should be remarked that for the tests with wave steepness $s_{op} = 0.04$ wave breaking occurred in the channel, where energy reduction is also incorporated in the reflection coefficient $\bar{R}(\infty)$.

The measured variation of $H_{m_0}(x)$ for the four tests is shown in Fig. 6, together with the variation according to linear wave theory. The theoretical values include wave shoaling and reflection effects according to (21) and (20). The wave conditions and reflection coefficients from Table 1 were used for the linear wave theory computations. The phase shift $\Delta\psi_r$ was assumed to be zero, and the reflection coefficient was assumed to be frequency-independent; $|R(f)| = \bar{R}(\infty)$. Although the measurements were for high waves including wave breaking, there is a good agreement between measurements and linear wave theory results. For a JONSWAP incident wave spectrum and a highly reflective structure such as the vertical wall in Tests 1 and 2, H_{m_0} only becomes more or less independent of the measuring position for x/λ_p larger than 2. For the breakwater, which has a lower reflection coefficient, single-gauge wave measurements can be done a little bit closer to the struc-

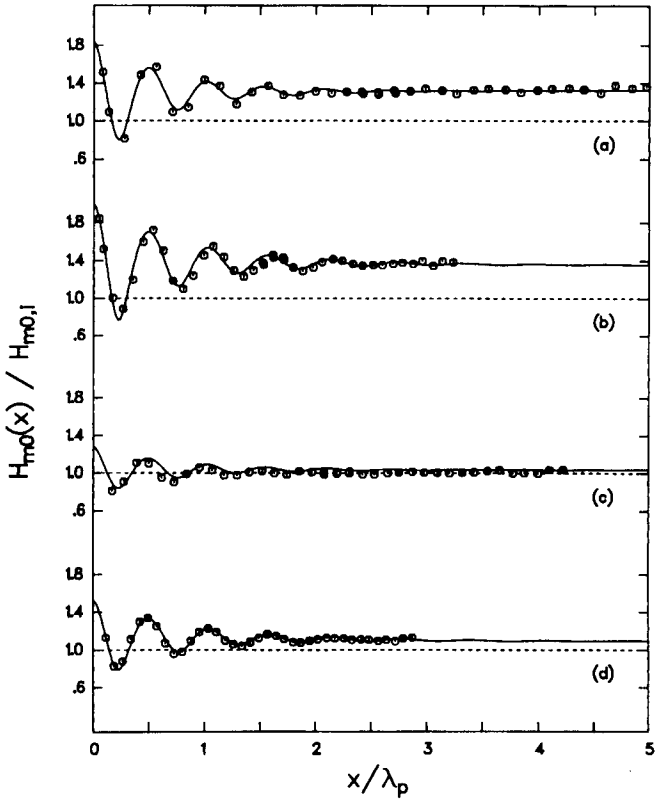

FIG. 6. Measured and Theoretical Variation of $H_{m_0}(x)/H_{m_0,I}$ as Function of x/λ_p: (a) Test 1, Vertical Wall and $s_{op} = 0.04$; (b) Test 2, Vertical Wall and $s_{op} = 0.02$; (c) Test 3, Breakwater and $s_{op} = 0.04$; (d) Test 4, Breakwater and $s_{op} = 0.02$ (——, Theory; ○, Experiment)

ture. In general it can be recommended to place wave gauges for single-gauge significant wave-height measurements further than two spectral-peak wavelengths away from the reflective structure for JONSWAP spectra. Goda (1985, Section 3.6) and Goda and Suzuki (1976) recommend a minimum distance of one λ_p from the structure, but the incident wave spectrum they used was much less narrow-banded than the JONSWAP spectrum we used. As shown in (30) the oscillations extend over a larger distance when the spectrum becomes more narrow-banded.

For Test 2, some wave spectra measured at different distances from the vertical wall are presented in Fig. 7. The same type of behavior can be seen as in Fig. 2 for linear wave theory, with nodes and antinodes at different frequencies, as explained before with the aid of linear wave theory. The decreased spacing of frequency nodes when moving away from the structure can clearly be seen.

The results of a multigauge wave analysis of incident and reflected waves are shown in Figs. 8 and 9. We analyzed the data in sets of three wave gauges, with the outer gauges located 0.8 and 0.4 m from the middle one, and the results plotted for the locations of the middle gauge. The multigauge analysis method used for the determination of incident and reflected waves is a least-squares technique similar to the one of Mansard and Funke (1980). This technique may be improved and extended to more gauges, as shown in Zelt and Skjelbreia (1992). Also techniques using combined velocity and/or surface elevation data for determining incident and reflected waves are feasible [see, e.g., Hughes (1993)]. Figs. 8 and 9 give the computed incident significant wave height $H_{m_0,i}(x)$ and reflection coefficient $\bar{R}(x)$ as a function of the distance to the structure x/λ_p. For Test 4 with a breakwater, the multigauge technique can be used up close to the structure, i.e., only for $x/\lambda_p < 0.4$ there seems to be an influence of the structure resulting in a light increase in $\bar{R}(x)$ and a small dip in $H_{m_0,i}(x)$. This may be due to the influence of evanescent wave modes near the structure, which are wave modes dying out fast exponentially when moving away from the structure [see, e.g., Dean and Dalrymple (1991, Section 6.3)]. The evanescent modes add to the pattern of incident and reflected waves and are not accounted for in the applied three-gauge technique. But nevertheless multigauge incident and reflected wave analysis can be used much nearer to the structure than would appear from the single-gauge analysis and measurements. For the vertical wall (Test 2) the multigauge technique can be used even closer to the structure: For $x/\lambda_p < 0.25$ a hardly significant dip in $H_{m_0,i}(x)$ and $\bar{R}(x)$ can be observed. This

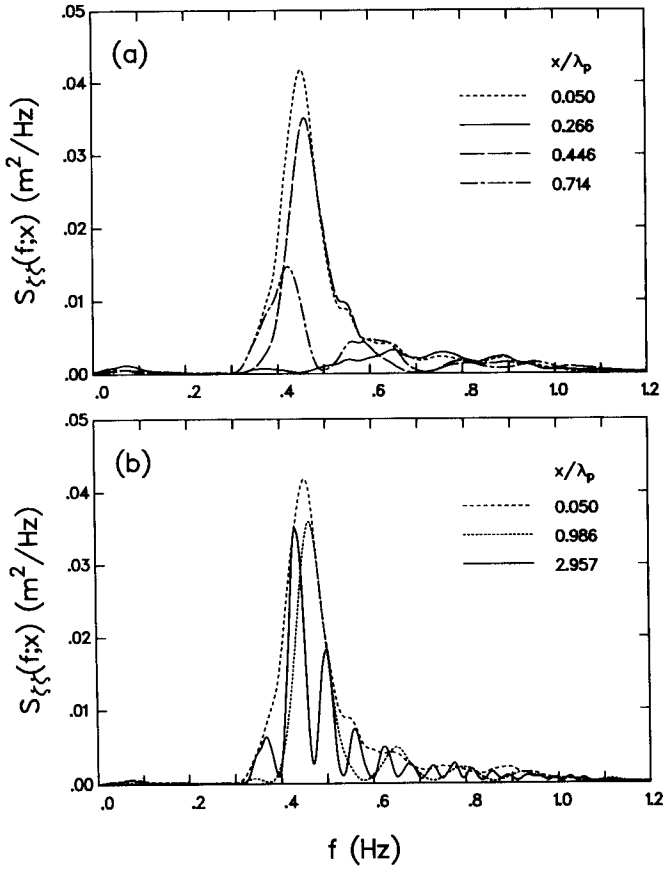

FIG. 7. Wave Spectra $S_{\zeta\zeta}(f; x)$ as Function of f/f_p for Test 2 at Different Locations

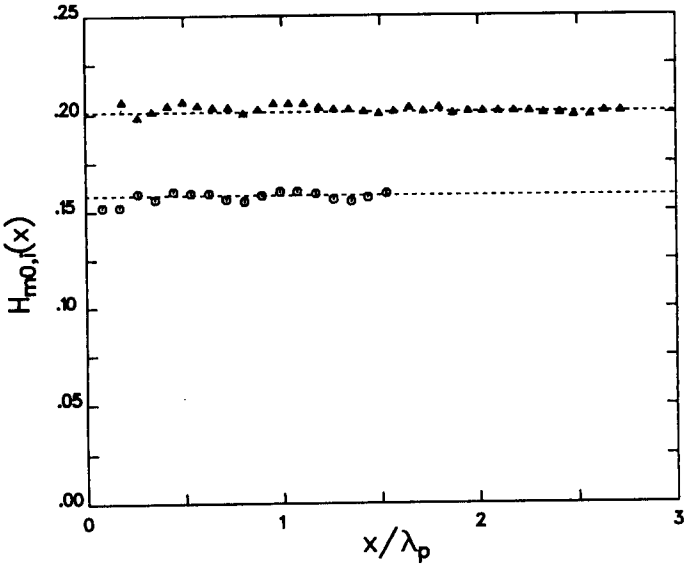

FIG. 8. Incident Significant Wave Height $H_{m_0,i}(x)$ as Function of x/λ_p, Determined from Measurements by Three-Gauge Wave Analysis: (a) ○, Test 2, Vertical Wall and $s_{op} = 0.02$; (b) ▲, Test 4, Breakwater and $s_{op} = 0.02$

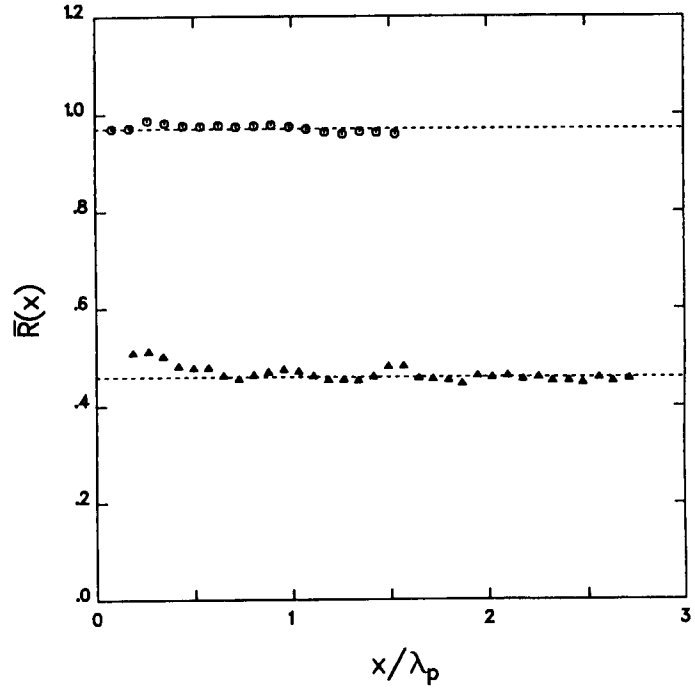

FIG. 9. Reflection Coefficient $\bar{R}(x)$ as Function of x/λ_p, Determined from Measurements by Three-Gauge Wave Analysis: (a) ○, Test 2, Vertical Wall and $s_{op} = 0.02$; (b) ▲, Test 4, Breakwater and $s_{op} = 0.02$

is due to the fact that near a perfectly reflective wall according to linear wave theory there are no evanescent wave modes, and only the incident and reflected traveling waves are present. These findings are in agreement with the results of Hughes (1993), who also found that incident and reflected waves could be determined with a technique using two orthogonal flow-velocity measurements.

CONCLUSIONS

The following conclusions with regard to the measurement of random waves in front of a reflective structure can be made:

1. From the measurements of the significant wave height $H_{m_0}(x)$, as well as from linear wave theory, a standing wave pattern in $H_{m_0}(x)$ shows up, extending over about two times the local spectral-peak wavelength λ_p for a JONSWAP incident wave spectrum. This is twice the distance that Goda (1985, Section 3.6) and Goda and Suzuki (1976) recommended, based on measurements with a spectrum less narrow-banded than the JONSWAP spectrum we used. This means that in laboratory experiments where only one wave gauge is used near the structure, it should be located far enough from the structure to be outside the region where $H_{m_0}(x)$ oscillates significantly.
2. Multigauge analysis of incident and reflected waves can be performed very close to the structure, the distance mainly being limited by the presence of evanescent wave modes near the structure. For the tested breakwater, and the wave conditions used, multigauge incident and reflected wave analysis results were independent of the distance to the structure for $x/\lambda_p > 0.4$.
3. Measured and theoretical wave spectra show a pattern of nodal and antinodal frequencies. The distance between nodal frequencies decreases for increasing offshore distance x.
4. Linear wave theory predicts a reduction of the distance over which the significant wave height $H_{m_0}(x)$ oscillates when the spectrum width increases. Long-crested incident waves show oscillations in $H_{m_0}(x)$ over a larger extend when the angle of incidence increases. Multidirectionality of the incident waves reduces the region of wave-height oscillations a bit for waves of normal incidence but significantly for waves of nonnormal incidence. For multidirectional waves with directional spreading $\sigma = 20°$ there is little difference in the region of wave-height oscillations for angles of incidence $\bar{\theta} = 0°$ and 30°, in contrast with the case of long-crested incident waves.

ACKNOWLEDGMENTS

This work has been undertaken by Delft Hydraulics as part of the MAST-2 Coastal Structures research program. It has been jointly funded by Delft Hydraulics and the Commission of the European Communities Directorate General XII for Science, Research and Development.

APPENDIX I. REFERENCES

Dean, R. G., and Dalrymple, R. A. (1991). *Water wave mechanics for engineers and scientists.* World Scientific, Singapore.

Dingemans, M. W. (1997). *Water wave propagation over uneven bottoms.* World Scientific, Singapore.

Goda, Y. (1985). *Random seas and design of maritime structures.* University of Tokyo Press, Tokyo.

Goda, Y., and Suzuki, Y. (1976). "Estimation of incident and reflected waves in random wave experiments." *Proc., 15th Int. Conf. Coast. Engrg.*, Vol. 1, ASCE, New York, 828–845.

Gradshteyn, I. S., and Ryzhik, I. M. (1980). *Table of integrals, series, and products.* Academic, San Diego.

Hughes, S. A. (1992). "Estimating wave-induced bottom velocities at vertical wall." *J. Wtrwy., Port, Coast., and Ocean Engrg.*, ASCE, 118(2), 175–192.

Hughes, S. A. (1993). "Laboratory wave reflection analysis using co-located gages." *Coast. Engrg.*, 20, 223–247.

Le Méhauté, B., and Wang, J. D. (1982). "Wave spectrum changes on sloped beach." *J. Wtrwy., Port, Coast., and Ocean Engrg.*, ASCE, 108(1), 33–47.

Mansard, E. P. D., and Funke, E. R. (1980). "The measurement of incident and reflected spectra using a least squares method." *Proc., 17th Int. Conf. Coast. Engrg.*, Vol. 1, ASCE, New York, 154–172.

Zelt, J. A., and Skjelbreia, J. E. (1992). "Estimating incident and reflected wave fields using an arbitrary number of wave gauges." *Proc., 23rd Int. Conf. Coast. Engrg.*, Vol. 1, ASCE, New York, 777–789.

APPENDIX II. NOTATION

The following symbols are used in this paper:

a = wave amplitude;
$C_{\eta\eta}$ = spatial autocorrelation function of η;
c = wave celerity = $2\pi f/k$;
c_g = wave group velocity = $2\pi[\partial f/\partial k]$;
D = directional spreading function;
F = directional integral in Eq. (34)];
f = frequency;
f_p = spectral-peak frequency;
f_1, f_2 = nodal frequencies;
g = gravitational acceleration constant;
H_{m_0} = significant wave height = $4\sqrt{m_0}$;
$H_{m_0,i}$ = significant wave height of incident waves;
h = water depth;
h_0 = water depth in case of horizontal bottom;
i = $\sqrt{-1}$;
K_r = transfer function between η and ζ;
k = length of wave-number vector = $\sqrt{k_x^2 + k_y^2}$;
k_x = x-component of wave-number vector;
k_y = y-component of wave-number vector;
m_0 = total variance of ζ;
n, n_1, n_2 = integer indices;
R = complex-valued reflection coefficient;
$\bar{R}$ = frequency-averaged reflection coefficient;
$|R|$ = absolute value of reflection coefficient;
Re = real part of following complex-valued expression;
$S_{\zeta\zeta}$ = autospectral frequency density of ζ;
$S_{\eta\eta}$ = autospectral frequency density of η;
s_{op} = wave steepness = $2\pi H_{m_0,i}/(gT_p^2)$;
T_p = wave period associated with spectral-peak frequency = $1/f_p$;
t = time;
x = horizontal cross-shore coordinate;
Y = y-coordinate of ray;
Y_0 = y-coordinate of ray passing through origin;
y = horizontal alongshore coordinate;
$\Gamma_{\eta\eta}$ = spatial autocorrelation function of η;
γ = peakedness parameter of JONSWAP spectrum;
$\Delta\psi$ = total phase difference;
$\Delta\psi_h$ = phase difference due to refraction and shoaling;
$\Delta\psi_r$ = phase difference due to reflection;
$\Delta\psi_y$ = phase difference between $(x, Y_0(x))$ and $(x, -Y_0(x))$;
δ = Kronecker delta function;
ζ = total free-surface elevation;
η = free-surface elevation of incident wave;
θ = angle of wave ray with negative x-axis;
$\bar{\theta}$ = mean wave direction;
θ_L = angle of wave ray for long-crested incident waves;
θ_0 = angle of wave ray at structure ($x = 0$);
λ_p = wave length associated with f_p and local water depth;
μ = $2kx\sigma^2 \cos\bar{\theta}$;
ν = $2kx\sigma^2 \sin\bar{\theta}$;
π = 3.14159 . . . ;
σ = directional-spreading standard deviation;
$\Phi_{\eta\eta}$ = autospectral wave-number density of η; and
ψ = wave phase.